NASA

Technical Memorandum **83818**

The Effect of Finite Field Size on Classification and Atmospheric Correction

Yoram J. Kaufman and Robert S. Fraser

SEPTEMBER 1981

National Aeronautics and Space Administration

Goddard Space Flight Center
Greenbelt, Maryland 20771

TM 83818

THE EFFECT OF FINITE FIELD SIZE ON CLASSIFICATION AND ATMOSPHERIC CORRECTION

Yoram J. Kaufman and Robert S. Fraser

Goddard Laboratory for Atmospheric Sciences

GODDARD SPACE FLIGHT CENTER
Greenbelt, Maryland 20771

ABSTRACT

The atmospheric effect on the upward radiance of sunlight scattered from the earth-atmosphere system is strongly influenced by the contrasts between fields and their sizes. For a given atmospheric turbidity, the atmospheric effect on classification of surface features is much stronger for nonuniform surfaces than for uniform surfaces. Therefore, the classification accuracy of agricultural fields and urban areas is dependent not only on the optical characteristics of the atmosphere, but also on the size of the surface elements to be classified and their contrasts. Atmospheric corrections that do not account for the nonuniformity of the surface have only a slight effect on the classification accuracy, in many cases, while in other cases the classification accuracy decreases. In this paper, the radiances above finite fields are computed to simulate radiances measured by a satellite. A simulation case including 11 agricultural fields and four natural fields (water, soil, savanah, and forest) is used to test the effect of the size of the background reflectance and the optical thickness of the atmosphere on the classification accuracy. It is concluded that new atmospheric correction methods, which take into account the finite size of the fields, have to be developed in order to improve significantly the classification accuracy.

CONTENTS

THE EFFECT OF FINITE FIELD SIZE ON CLASSIFICATION AND ATMOSPHERIC CORRECTION

1. INTRODUCTION

Efforts have been increasing during the last decade towards applying satellite images of the earth to classify and analyze surface features. These programs have been successful enough to encourage development of improved satellite sensors such as the Thematic Mapper and the Multispectral Resource Sampler (Schnetzler and Thompson, 1980). The earth's atmosphere has a significant bearing on the interpretation of the images. The initial studies of scattering and absorption effects in cloudless atmospheres assumed that the surface was uniform (Herman and Browning, 1975; Otterman and Fraser, 1976; Fraser et al., 1977; and Horvath et al., 1980). Attempts were made to develop corrections, again assuming that the surface was uniform (Turner, 1972; Fraser, 1974; Potter, 1976; Turner, 1978; and Slater, 1980). These methods depended on values of the aerosol optical thickness, which has been measured from satellites with success over large bodies of water (Griggs, 1973, 1974, and 1979; Mekler et al., 1977), surfaces with discontinuities in reflectance (Kaufman and Joseph, 1981), but unsuccessfully over land. Pearce (1977) showed, however, that nonuniform surface reflectance patterns outside of an instantaneous- field-of-view (IFOV) modify the effect of the atmosphere on the radiance, (see also Kawata et al., 1978; Haba et al., 1979; Otterman and Fraser, 1979; Mekler and Kaufman, 1980; and Dave, 1980). Schowengerdt and Slater (1979) recently concluded that the influence of neighboring pixels causes only a secondary

atmospheric effect. In the works of Kawata et al. (1978), Haba et al. (1979), and Kaufman and Joseph (1981), atmospheric corrections were applied, taking into account the finite size of the fields. From the Monte Carlo calculations of Pearce (1977), or from the approximate calculations of Mekler and Kaufman (1980), it is clear that the atmospheric effect is much stronger in the case of finite fields, than in the case of infinite fields (for the same atmospheric conditions) and thus, it is definitely not a secondary effect but a primary effect, wherever significant contrasts in surface reflectance exist.

The purpose of the present work is to show that classification errors are usually much bigger in regions consisting of finite fields of dimensions less than a few kilometers compared to errors where the fields are larger. In order to make accurate classification, the measured radiance should be corrected for the atmospheric effect. Atmospheric corrections that do not take into account the finite size of the fields, reduce the radiance errors slightly in most of the cases, in some of the cases the correction increases the error, and in the remaining few cases, the correction is satisfactory.

The radiances given here are computed only for the nadir, for nonabsorbing atmospheres, for the visible through near infrared spectral band (400 nm $\leq \lambda \leq$ 1100 nm), and for a total normal optical thickness of $\tau_o \leq 1.0$. Each portion of the earth's surface is assumed to reflect light isotropically according to Lambert's law. The term "field" here shall apply to either the test or the reference area, which is of uniform reflectance (e.g. a corn field a lake or an urban area). The background is the region surrounding the field.

The topics that follow are arranged such that the basic surface reflectance characteristics of finite fields are reviewed in section 2. Then a discussion of the atmospheric effects associated with finite fields follows in section 3. These effects cause errors in the derived radiances and attempts to make corrections without accounting for the surface nonuniformity are discussed in section 4. Section 5 contains a study of the classification errors in nonuniform regions. The conclusions are given in section 6. Appendix 1 gives a list of the notations. The equations used in these calculations are explained in the other appendices.

2. SURFACE AND ATMOSPHERIC CHARACTERISTICS

A. Surface reflectance

Statistics of the size of agricultural fields and water bodies were recently reported by Pitts and Badhwar (1980). They showed that the peak of the distribution of field size (including all crops) occurs for a size of 6 acres (corresponding to a square of edge length of 155 m), while 50 percent of the crop area is in fields smaller than 130 acres (corresponding to a square of edge length of 720 m). Therefore, a representative field-edge-length is of the order of one tenth to a few kilometers. For such surface cover, it is necessary to use atmospheric models which account for the finite size of the underlying fields. Figure 1 shows an example of the variations in the surface reflectance, taken by a Thematic Mapper simulator (Labovitz et al., 1980), and kindly given to us by D. L. Toll. The image of Fig. 1

ORIGINAL PAGE
BLACK AND WHITE PHOTOGRAPH

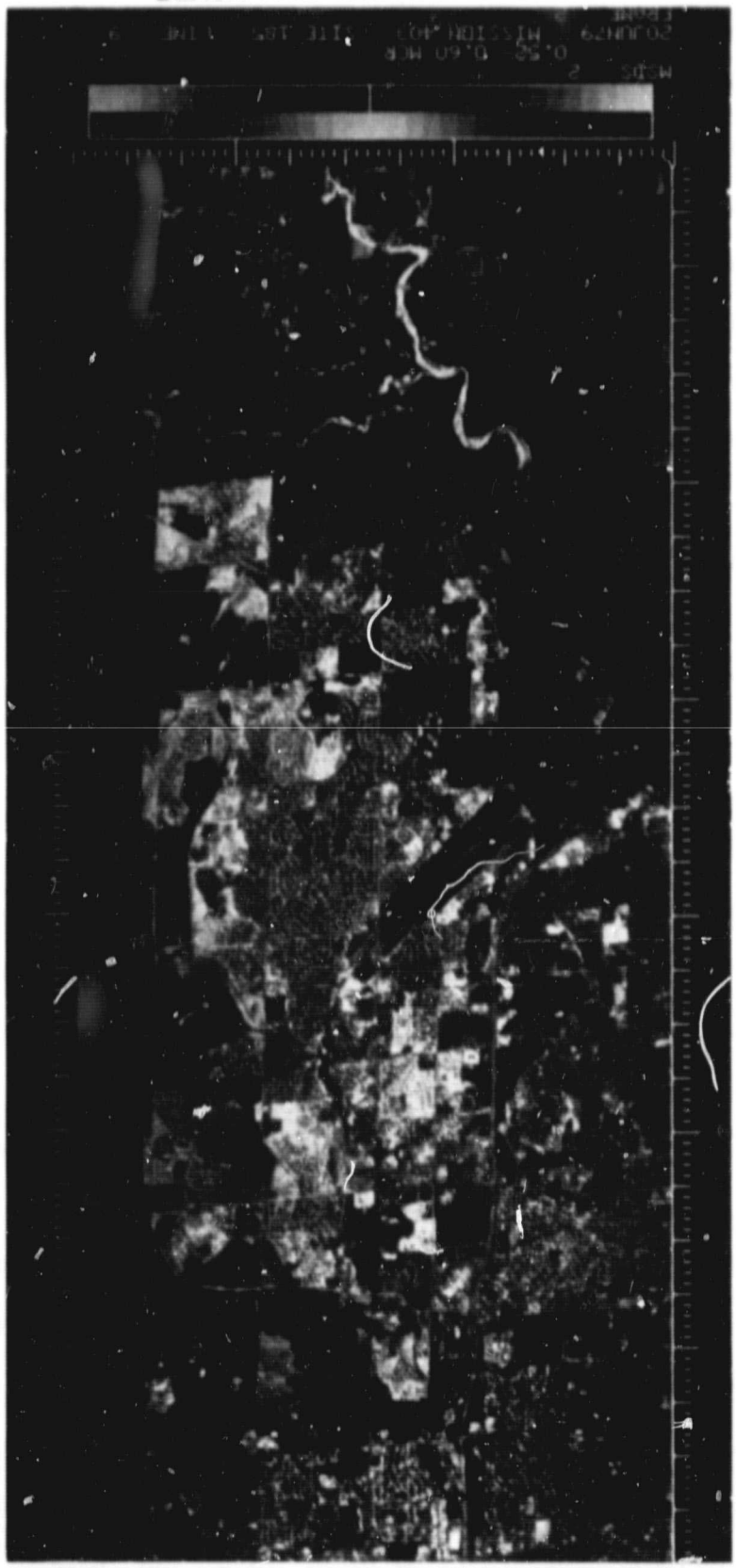

Figure 1. An image of the eastern fringes of Denver, Colorado, acquired by a Thematic Mapper simulator shows the high nonuniformity of the surface. The area size is 4 x 8 km. The wavelength is 450–520 nm, and the time is 1300 MDT (1900 GMT).

was acquired on the plains at the eastern fringe of Denver, Colorado. The flight took place on June 20, 1979, starting at 1:00 P.M. MDT (1900 GMT). The image is taken in the 450-520 nm band. The underlying surface is an urban and rural area. The image size is 4 x 8 km; the size of the fields range between a few tenths to a few hundred meters.

Figure 2 shows the probability of reflectivity of the data given in Fig. 1, in four bands (450-520 nm, 520-600 nm, 630-690 nm, and 760-900 nm). The range of the reflectance extends from 0.02 to 0.34. The reflectance was calculated by using laboratory calibration of the instrument (Richard, 1979 and 1981).

B. Atmospheric characteristics

The atmospheric optical characteristics depend strongly on the aerosol optical thickness. Flowers et al. (1969) reported the results of a five year study of atmospheric optical thickness measurements in the United States. They found for a wavelength of 500 nm that in most of the cases the aerosol optical thickness for rural regions was in the range $0.1 \leq \tau_A \leq 0.2$, for suburban regions in the range $0.1 \leq \tau_A \leq 0.3$, and for urban regions $0.4 \leq \tau_A$. A recent study (Pearson et al., 1981) analyzed turbidity data for 6 years from a non-urban area in North Carolina and showed an average optical thickness of $\tau_A = 0.3$. The summer average was about $\tau_A = 0.6$. These results show the high turbidities in the eastern U.S.

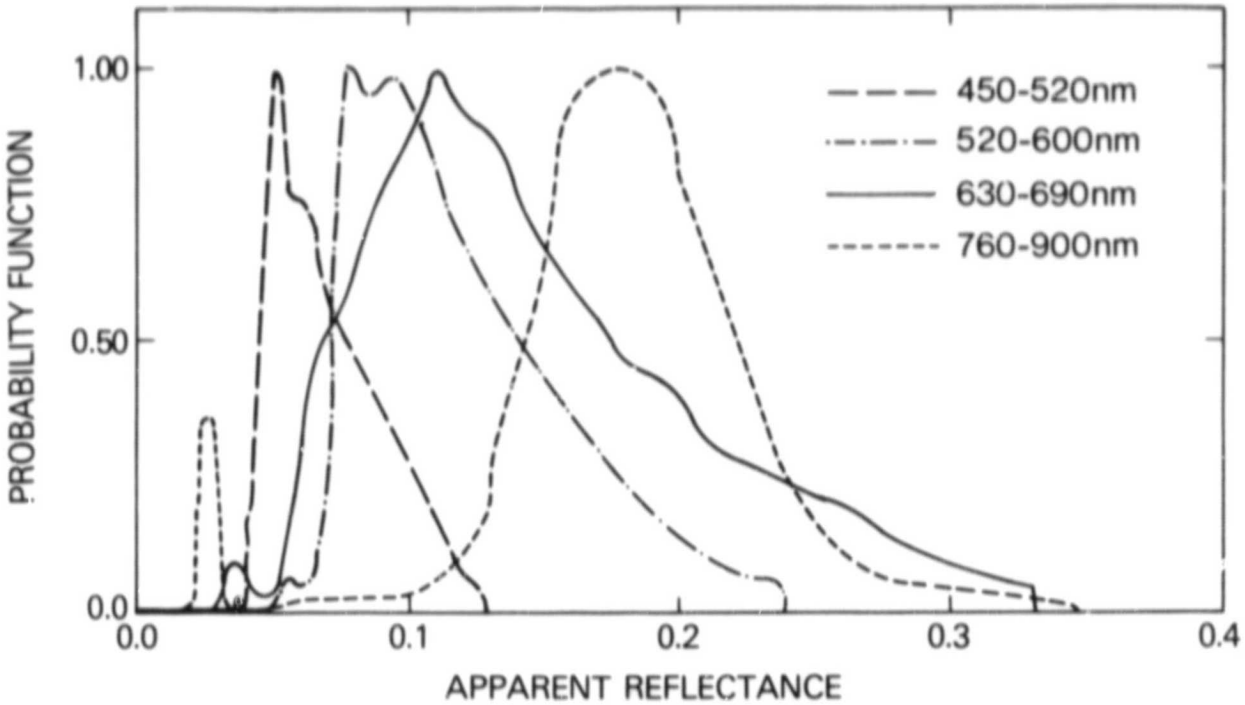

Figure 2. The probability of reflectivity of the data from the image on Figure 1 in four bands.

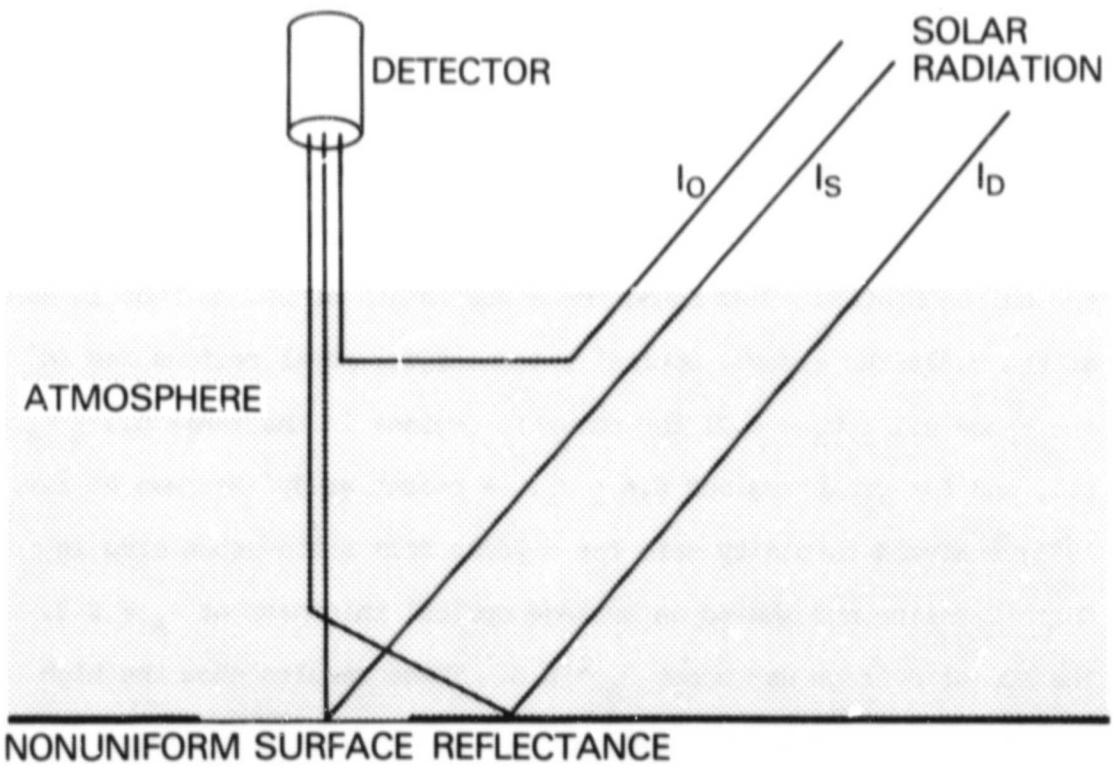

Figure 3. Schematic diagram of the contributions to the upward radiance.

3. THE EFFECT OF THE FINITE SIZE

In order to discuss the effect of nonuniform surfaces on the radiance measured at a satellite, it is convenient to use a normalized radiance (I), equivalent to the apparent reflectance, which is related to absolute radiance (I*) by

$$I = \pi I^* / (\mu_o F_o),$$

where $\mu_o = \cos \theta_o$, θ_o is the zenith angle of the sun; and F_o is the solar spectral irradiance above the atmosphere on a unit area perpendicular to the beam. The radiance of light reflected from the earth and its atmosphere is composed of three components (see Fig. 3):

$$I = I_O + I_S + I_D \qquad (1)$$

where,

I_O - radiance of light scattered from the direct sun beam into the detector's field-of-view without being scattered by the surface. This component is independent of surface reflectance and causes a loss of contrast on the satellite image.

I_S - radiance of light reflected by the observed field and directly transmitted through the atmosphere. This component is the attenuated signal, the measurement of which gives

remote sensing information about the surface.

I_D - radiance of light reflected from the field and its background and then is scattered by the atmosphere to the detector. This component modifies the apparent spectral signature of the observed field and reduces the contrast between it and the adjacent region.

The difference between the atmospheric effect for uniform and nonuniform surface reflectance can be explained by means of these three components. Since the term I_0 is independent of surface reflectance, it is the same for the uniform and nonuniform surfaces. The term I_S is dependent mainly on the reflectivity of the observed field and therefore is almost the same for uniform and nonuniform surfaces. The expression for I_S can be deduced from Chandrasekhar (1960, Eq. 201), where the explicit dependence of the upward radiance on the surface reflectance is given. The resultant expression is:

$$I_S = \frac{\gamma_o \, e^{-\tau_o}}{1 - \ell A_a} \, A_S \qquad (2)$$

where γ_o is the total (diffuse and direct) transmission of the sunlight to the surface, τ_o is the total atmospheric optical thickness (aerosols and molecules) A_S is the reflectivity of the field, and $(1 - \ell A_a)$ accounts for the contribution of multiple scattering of light between the surface and the atmosphere. The reflectance A_a is an average of the reflectance of the field and the reflectance of its

background. Since the term (ℓA_a) is usually small, $\ell A_a \ll 1$ (for τ_o = 0.35, λ = 550 nm, and A_a = 0.2; ℓA_a = 0.025). I_S depends mainly on A_S rather than on the size of the field and the reflectance of its background.

The difference between the atmospheric effect for uniform and nonuniform surfaces is expressed by the diffuse radiance, which is also deduced from Chandrasekhar (1960):

$$I_D = \frac{\gamma_o D}{1 - \ell A_a} \tag{3}$$

where D is the diffuse transmission through the atmosphere, rather than direct transmission from the surface to the detector; A_D is a weighted average (different from A_a) of the surface reflectance of the entire surface, including the observed field and its surrounding. For a uniform surface, boch the field and its background are assumed to have the same reflectance, while in the nonuniform case, they have a different reflectance, resulting in different effects on the measured radiances. The values of A_a and A_D can in principle be computed by solving the equation of radiative transfer for the nonuniform surface. In the present work, the values are derived from Monte Carlo computations.

The term adjacency effect specifies the influence of nonuniform areas on the radiance and is defined by the difference between radiances above uniform (I^u) and nonuniform (I^n) surface:

$$\delta I^A = I^n (A_f, A_B, T) - I^u (A_f, A_f, T) \quad (4)$$

Here, A_f and A_B are the reflectances of the observed field and its background, respectively. T is the atmospheric turbidity. Hence, the adjacency effect is zero for a uniform surface, negative for a darker background, and postivie for a brighter background.

The effect of a change in the atmospheric haziness on the detected radiance for uniform and nonuniform surfaces can be seen in Fig. 4. This figure gives a schematic representation of the changes in the three components of the radiance, for three different cases of background reflectance relative to the field reflectance: (a) background much brighter than the field, (b) uniform surface (same brightness of the field and the background), and (c) darker background. The effect of the atmosphere on two of the components, I_O and I_S, is the same in all of the cases. The diffuse radiance I_D decreases as the background reflectance decreases. The bright background in Fig. 4a causes a strong increase in the total radiance (I) with the optical thickness. The increase is moderate in Fig. 4b, and the dark background in Fig. 4c causes a decrease in the radiance with the optical thickness. We conclude from this discussion that for the same atmosphere the radiance may increase or decrease, depending on the relative brightness of the field and its background. This phenomena can not be predicted by an atmospheric model that is based on the assumption of uniform surface reflectance.

Figure 5 shows the results of Pearce's (1977) Monte Carlo

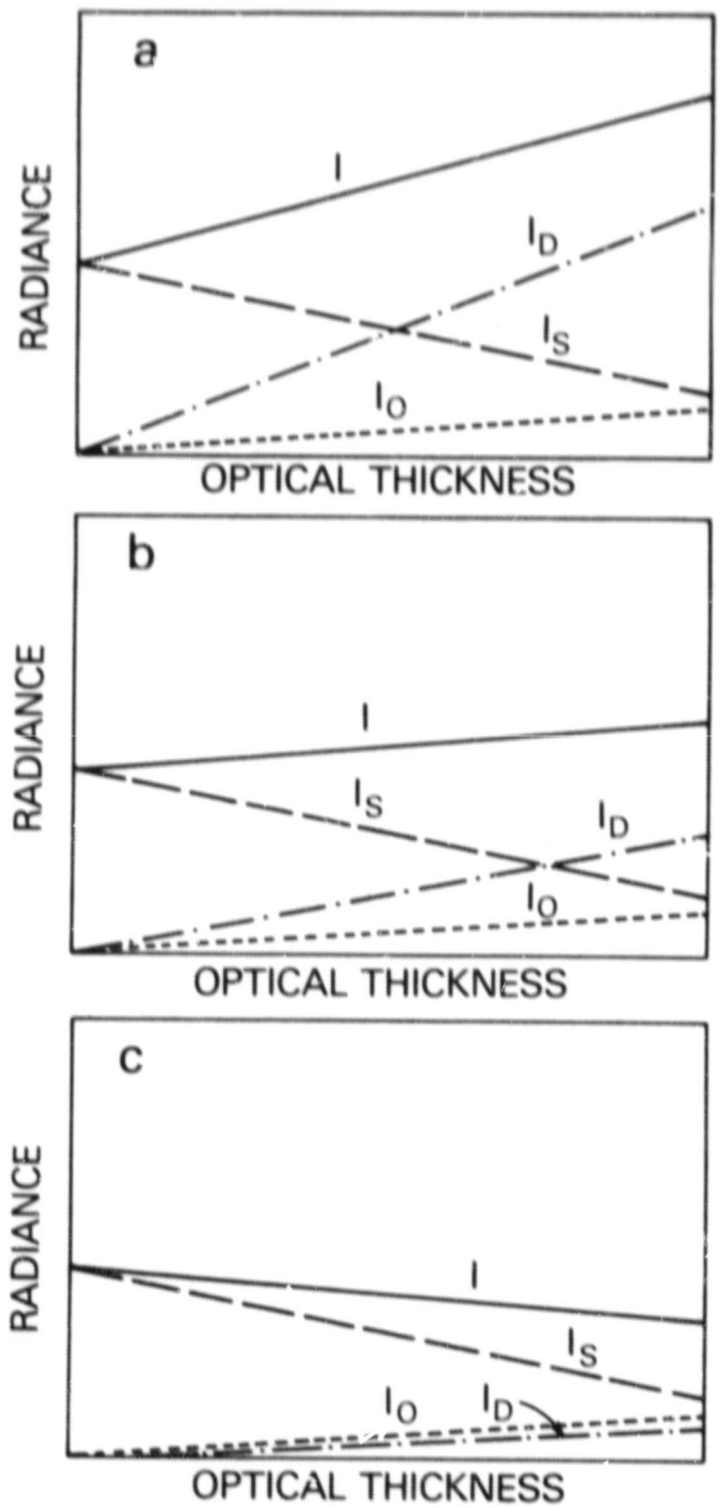

Figure 4. Schematic diagram of the atmospheric effect on the upward radiance. Both the radiance and the optical thickness are given in arbitrary units: (a) the background is much brighter than the classified area; (b) uniform surface (same brightness), and (c) the background is much darker.

computations of the nadir radiance above the center of a square surrounded by a different background (the IFOV is 30 m). The reflectance of the square is $A_S = 0.4$ for the upper three curves, while the background is of reflectance $A_B = 0.2$. For the lower three curves, the square is of reflectance 0.2, while the background is of reflectance $A_S = 0.4$. In this figure, the radiance is shown as a function of the edge length of the square. The atmosphere is nonabsorbing and is modeled with three different aerosol optical thicknesses (0.0, 0.213, and 0.638), corresponding to turbidities (0, N, and 3N), respectively. The aerosol size distribution is given by Pearce (1977). The index of reflectance is $m = 1.5 + 0.0i$. The asymptotic values of the radiances are given on the right side for each case. It is seen that a change in the atmospheric turbidity from 0 to 3N causes an increase in the radiance by 4 percent for an infinite square (uniform surface), while for a finite square (of reflectance $A_S = 0.4$ on background of reflectance $A_B = 0.2$) of edge length of 0.3 km, the effect is to reduce the radiance 15 percent when the aerosol optical thickness is increased from (0.0) to (0.638). This comparison emphasizes that the atmospheric effect is different for finite fields than for infinite fields. Figure 6 shows similar results for a square and background of reflectances 0.0 and 0.6, respectively. This figure and Fig. 5 are used for the computations in this paper.

In order to increase our confidence in the results of Figs. 5 and 6, the results of the Monte Carlo computations are compared to exact numerical results based on codes developed by Dave (1970) for a

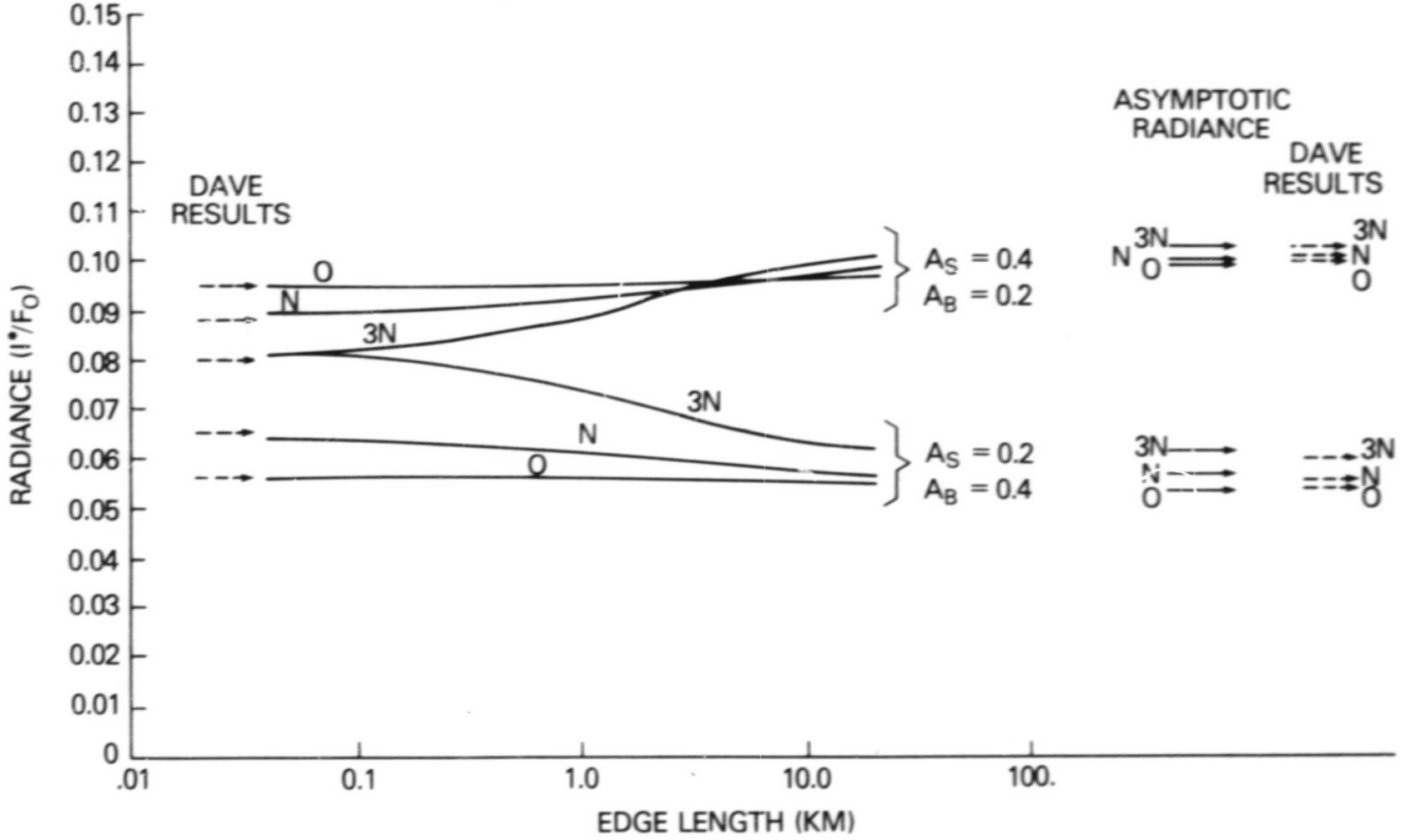

Figure 5. Upward radiance at the nadir above the center of a square as function of the edge length of the square (after Pearce, 1977). The atmospheric turbidity is given for each curve. The wavelength is 550 nm. The square reflectivity (field albedo) (A_S) and the background reflectance (A_B) are given for each group of curves. The asymptotic radiance and the radiance for infinitesimal square are compared with exact computations according to Dave's code (dashed arrows).

uniform surface. The comparison was performed for the asymptotic radiances and for an infinitesimal square on a large background. In the later case, the results of Dave were used with the aid of equations given in Appendix 2. Most of Dave's calculations agree with the Monte Carlo results of Pearce (1977) with a difference of less than 2 percent. The Monte Carlo results were also compared with an analytical approximate solution by Mekler and Kaufman (1980), resulting in similar good agreement. Therefore, the results of Figs. 5 and 6, and similar data given by Pearce (1977) are used in the following analyses with confidence in their accuracy. In order to use these computational results for different values of surface reflectance, the radiance transformations, explained in Appendix 3, are applied.

4. THE CHANGE IN RADIANCE

In this section we shall analyze the changes in the radiance used for classification due to the atmospheric effect in the case of finite fields. The classification is performed by comparing the radiance of the test area (I_t) with the radiance above the reference area (I_r). We shall use the following notation for the radiance I_i (A_i, A_{Bi}, T_i, X_i), where i can be t or r; A_i is the reflectivity of a square (the reference or test area), A_{Bi} is the reflectivity of the background, T_i is the atmospheric turbidity, and X_i is the edge length of the area. Thus, the radiance above the center of the reference area in Fig. 7, for example, is I_r (0.2, 0.1, 1, 0.29). The relative change in radiance is calculated by:

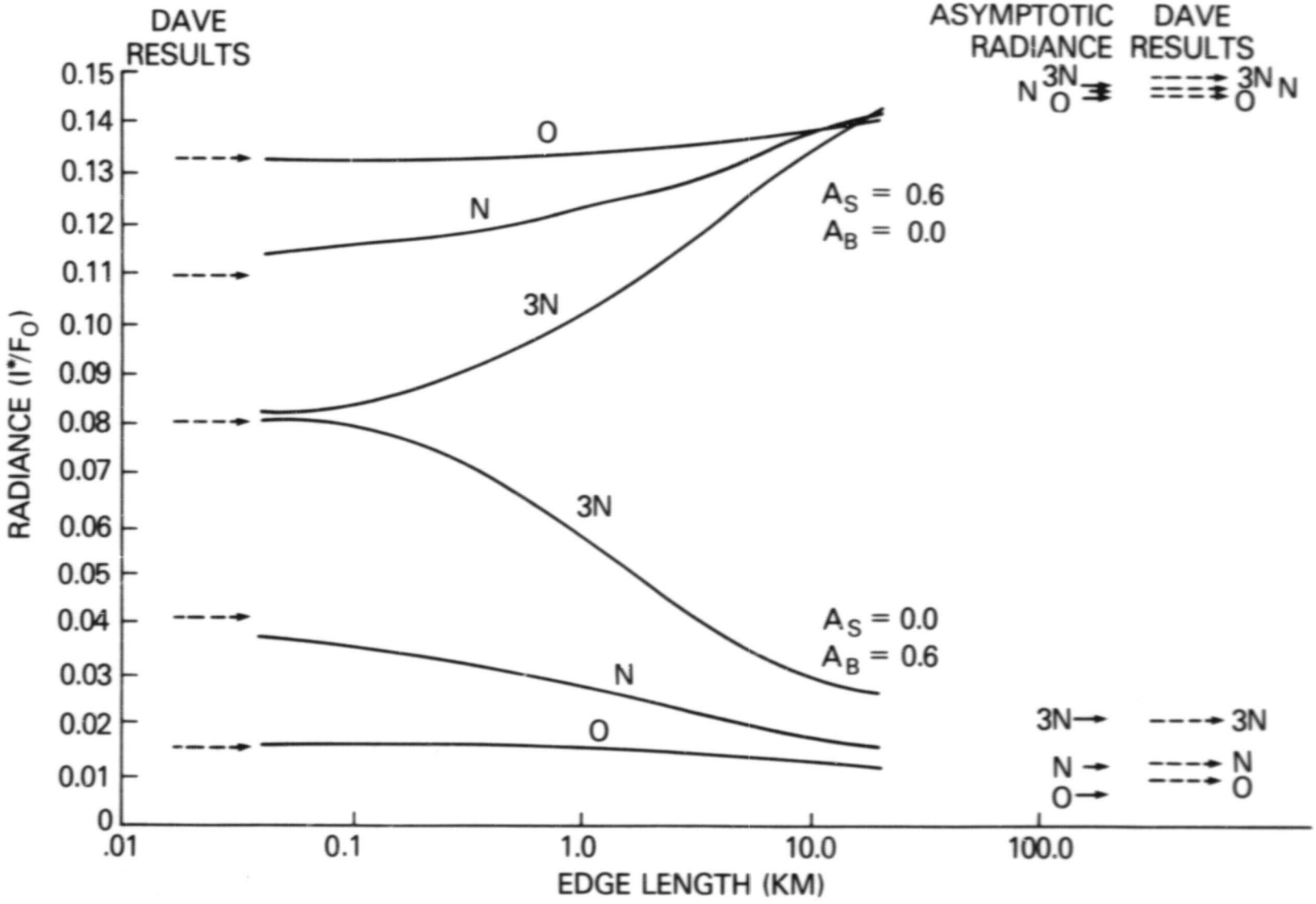

Figure 6. Same as Figure 5, but for a different couple of square and background reflectivity.

$$\frac{\Delta I}{I_e} = \frac{I_t\ (A_t,\ A_{Bt},\ T_t,\ X_t) - I_r\ (A_r,\ A_{Br},\ T_r,\ X_r)}{I_e\ (A_t)} \qquad (5)$$

where $I_e\ (A_t)$ is the radiance which would be measured above an area of reflectivity A_t, when no atmosphere is present. We shall always use the same reflectivity for the reference area and for the test area ($A_r = A_t$) in all following examples; thus without an atmospheric effect, we would expect $\Delta I = 0$.

The effect of size and background reflectance on the error in radiance is examined in Fig. 7. The surface and atmospheric characteristics of the reference area are the same in Figs. 7 and 8: $A_r = 0.2$, but its background reflectance $A_{Br} = 0.1$, $X_r = 0.29$ km, and $T_r = 1$. The atmospheric turbidity is the same for the test area and the reference areas in Fig. 7. Therefore, without an effect due to the finite sizes of the fields, the difference in the radiance would be zero. It is seen that for the same background ($A_{Bt} = 0.1$), the difference in the radiance for a small test area ($X_t \leq 2$ km), is small ($|\frac{\Delta I}{I_e}| \leq 0.025$) but reaches ($\frac{\Delta I}{I_e} = 0.075$) for an infinite test area. For high reflectance of the background ($A_{Bt} = 0.4$), the difference reaches (0.25), while for a black background ($A_{Bt} = 0$), the difference reaches (-0.10). An atmospheric correction, which ignores the finite size of the fields, even if taking into account exactly all atmospheric optical characteristics, would not perform any correction on the data of Fig. 7, since the atmospheric optical thickness is the same for the test area and the reference areas.

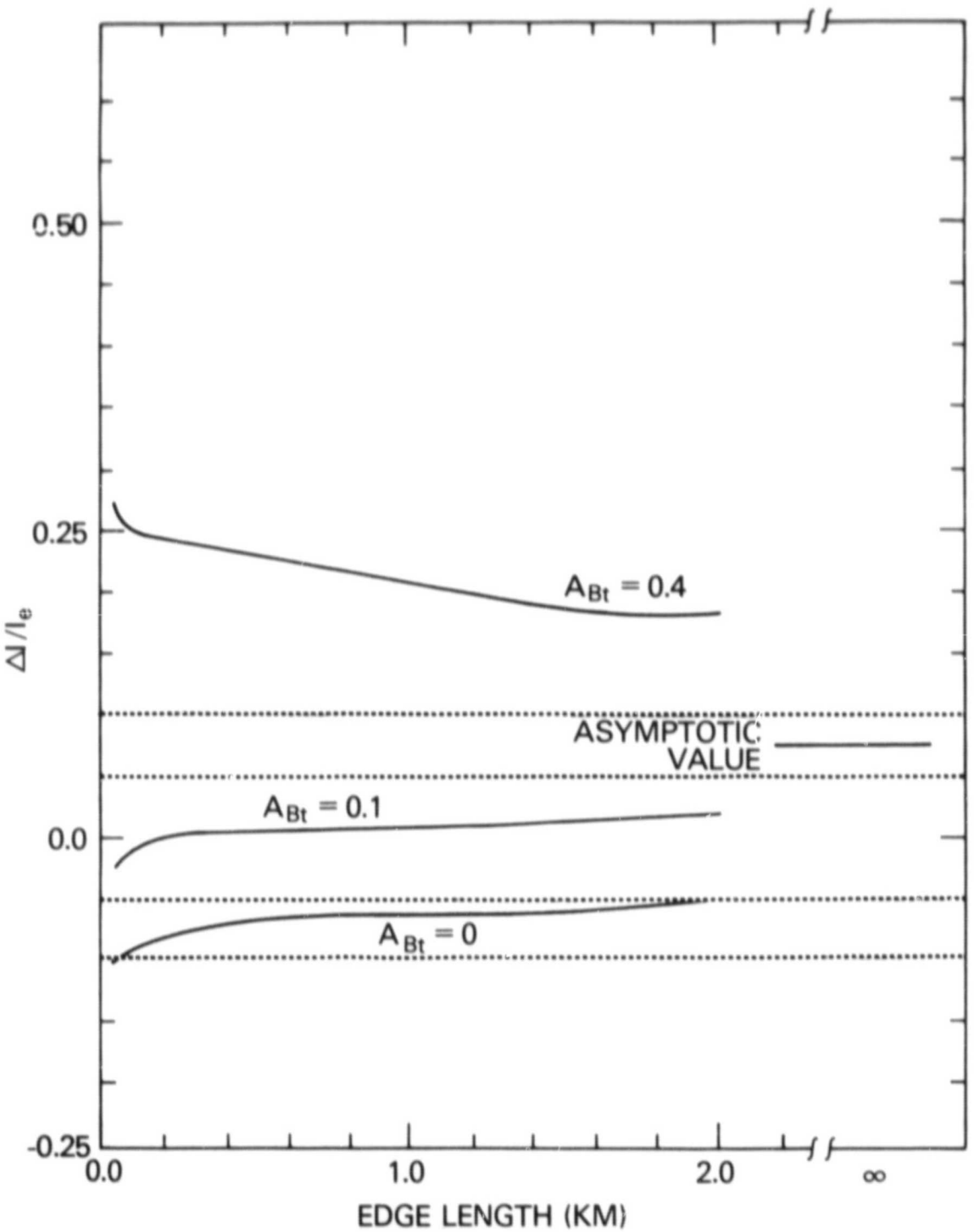

Figure 7. The relative difference in radiances (solid lines) of the test and reference areas $(I_t - I_r)/I_e$ as a function of the length of the test square side (abscissa) and of the reflectance of the background (A_{Bt}) surrounding the test square. The reference and test area have the same reflectance of $A_r = A_t = 0.2$, but the reflectance of the background to the reference area is $A_{Br} = 0.1$. The reference area's edge length is $X = 0.29$ km. The atmospheric turbidity is the same for the reference and test areas ($T_r = T_t = 1$). The dotted lines give the tolerances for the difference in radiance for classification purposes.

Two tolerance differences in radiances are introduced in Fig. 7, as well as in all other figures giving results for the difference in radiance. These two tolerances are representative for the maximum difference in the radiance for which classification is still possible (assuming there are no other sources of errors). In this case, the two tolerance values of $\pm$ 0.05 and $\pm$ 0.10 are chosen as the representative class separation in the classification examples given in section 5 of this paper. With such tolerance limits, correct classifications can be made when the background reflectance is 0.1 but not for 0.4 (Fig. 7).

The relative difference of radiances, when the reference and test fields are subject to different atmospheric turbidities is shown in Fig. 8. The turbidities for the test and reference areas are $T_t = 3$ and $T_r = 1$. When the backgrounds to the test and reference areas have the same reflectances ($A_{Bt} = A_{Br} = 0.1$), the relative difference in radiances ranges between -0.01 to 0.06 for fields smaller than 2 km. The magnitude of the radiance difference jumps to the 0.3 to 0.6 range for a large difference in the background reflectances ($A_{B'} = 0.4$).

The atmospheric corrections used in Fig. 8 for the uniform surface were derived from Fig. 9. There the upward radiance at nadir above a uniform surface of reflectance (A) was plotted for the three atmospheric turbidities used in Figs. 5-8. The results shown on Fig. 9 were calculated by Dave's routine for the same atmospheric characteristics that were used for the Monte Carlo computations. For "measured" radiance and turbidities appearing in Fig. 8, the

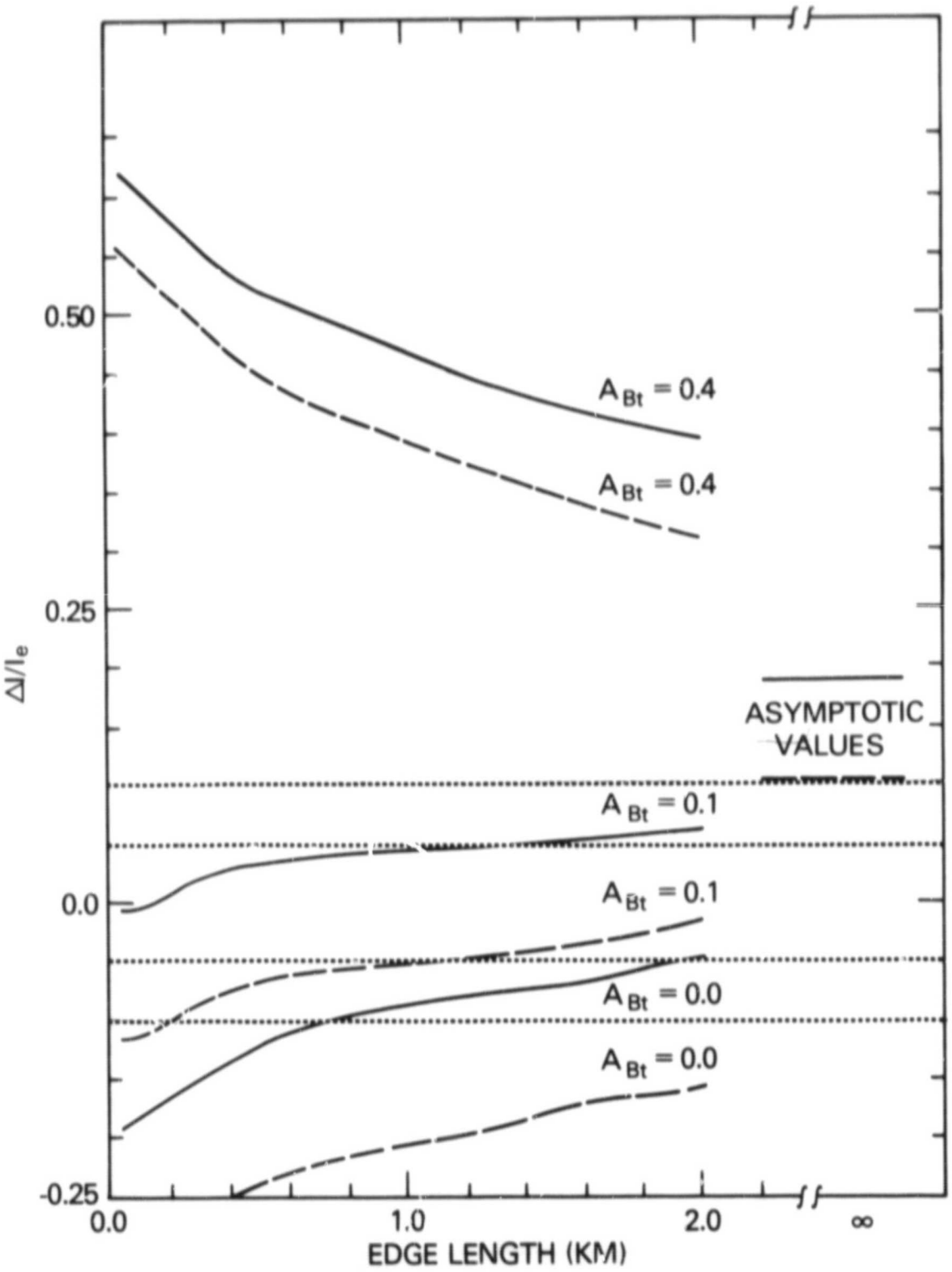

Figure 8. Same as in Figure 7, but for different atmospheric turbidity of the test and reference areas ($T_r = 1$, $T_t = 3$). The solid lines give the relative difference in radiance without any atmospheric correction, and the dashed lines give the difference with atmospheric corrections that ignore the finite size of the fields. The dotted lines are the same as in Figure 7.

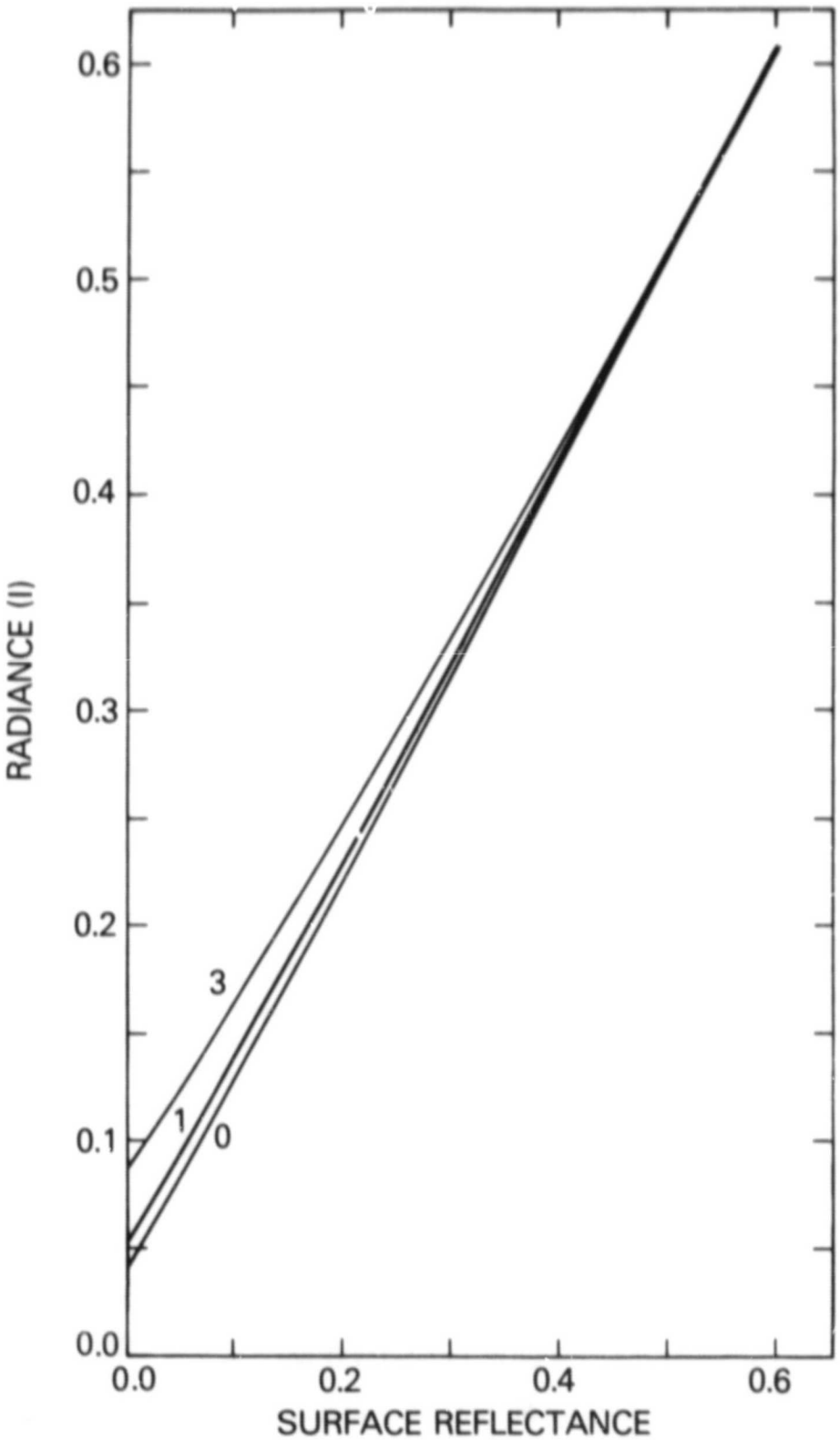

Figure 9. The upward radiance at the nadir for a uniform surface of reflectance (A) and for the three atmospheric turbidities.

corresponding radiance for unit turbidity (T = 1) was found from the curves in Fig. 9. The atmospheric correction applied here (dashed lines in Fig. 8), corrects slightly the radiance for $A_{Bt} = 0.4$, while increasing the magnitude of the difference for $A_{Bt} = 0.0$, and having a mixed effect for $A_{Bt} = 0.1$.

The effect of the background reflectance on the change in the radiance is shown in Fig. 10. It is seen that the relative difference increases almost linearly as the background reflectance departs from the value of A_t. This linearity can be demonstrated with the previous equations by first substituting Eqs. (2) and (3) in (1) to find the radiance above a nonuniform surface:

$$I = I_o + \frac{\gamma_o}{1 - \ell A_{ai}} \left(e^{-\tau_o} A_i + DA_{Di}\right), \quad i = t, r. \tag{6}$$

The relative difference in the radiance above test and reference areas is given by:

$$\frac{\Delta I}{I_e} = \frac{\gamma_o \left(e^{-\tau_o} A_t + DA_{Dt}\right)}{1 - \ell A_{at}} - \frac{\gamma_o \left(e^{-\tau_o} A_t + DA_{Dr}\right)}{1 - \ell A_{ar}} \tag{7}$$

where the reflectances of the test and reference areas are the same ($A_t = A_r$), but their background reflectances differ. Since $\ell A_{at} \ll 1$ and $\ell A_{ar} \ll 1$, the difference is close to:

$$\frac{\Delta I}{I_e} \approx \gamma_o D \left(A_{Dt} - A_{Dr}\right) \tag{8}$$

As a result of the average reflectances A_{Dt} (for the region of the

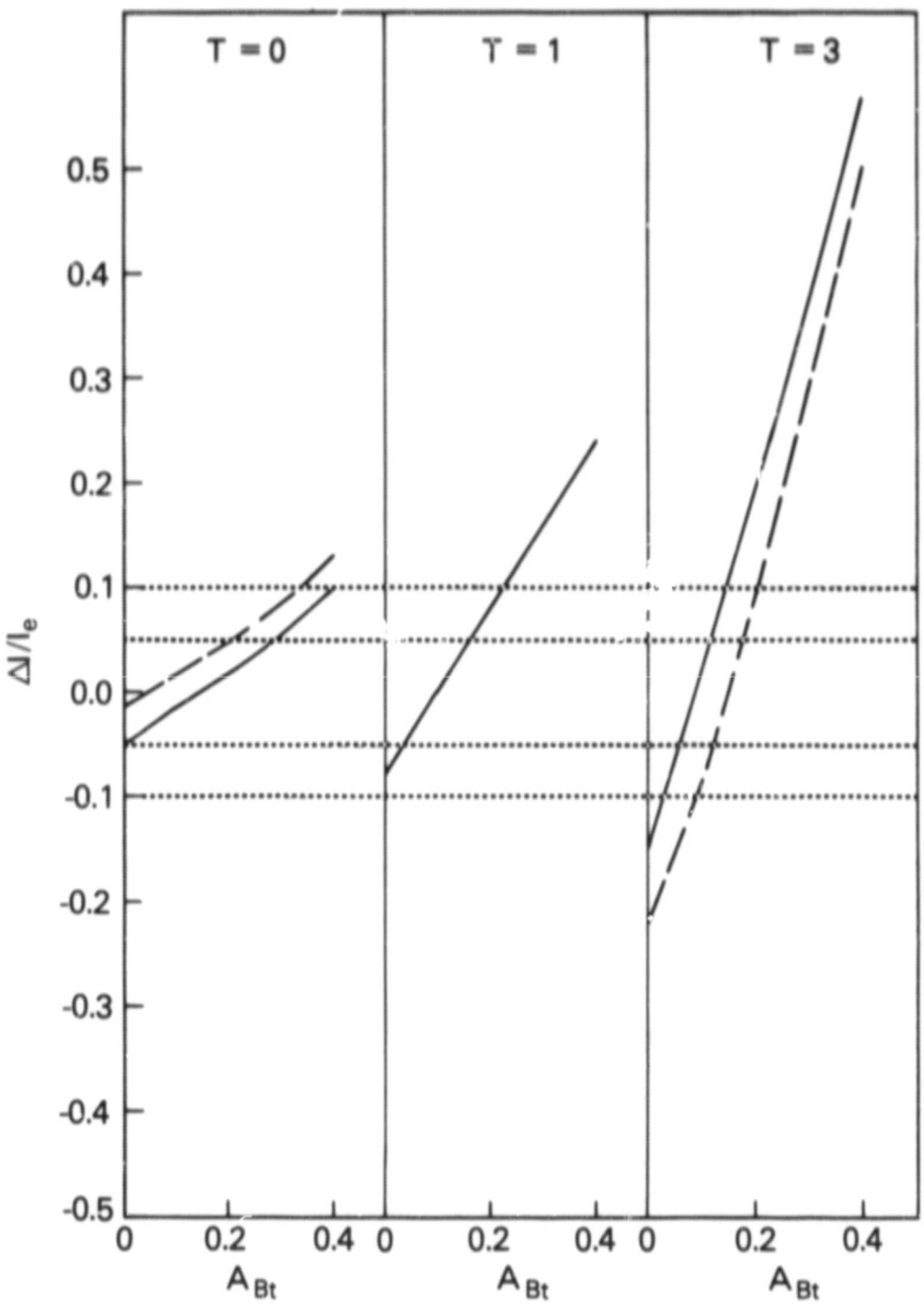

Figure 10. The relative change in radiance as a function of background reflectance (A_{Bt}), for the three atmospheric turbidities. A solid line gives results for no atmospheric correction, and a dashed line gives results with uniform atmospheric correction. Both the test and reference areas are of edge length $X_t = X_r = 0.29$ km, and $A_t = A_r = 0.2$. The background reflectivity of the reference is $A_{Br} = 0.1$. The dotted lines give the ±5 and ±10% tolerance values of the difference in radiance. Note that for T = 1, the dashed line matches the solid line.

test square) and A_{Dr} (for the reference square) being linearly dependent on their background reflectance, the linear dependence of the difference between radiances (ΔI) follows:

$$\frac{\Delta I}{I_e} \approx \gamma_o D \, (A_{Bt} - A_{Br}) \tag{9}$$

The atmospheric correction, based on a uniform surface, is shown by the dashed lines in Fig. 10. The atmospheric correction, while having no effect for T = 1, decreases the radiances for T = 0 and increases them for T = 3.

When the turbidity = 3, the corrected intensities lie within the $\pm$ 5 percent tolerance limits only for $0.12 < A_{Bt} < 0.18$. The difference between radiances for the test and reference fields for additional permutations of their parameters is plotted as a function of the aerosol optical thickness in Fig. 11. The continuous lines show the relative difference. The dashed lines result after the test radiances are corrected for atmosperic effects that are based on the assumption that the surface reflectance is uniformly the same as for the test field. The reflectances of the reference and test fields are the same. The reference parameters are constant ($A_r = 0.2$, $A_{Br} = 0.1$ $X_r = 0.29$ km, and $T_r = 1$).

Only the background reflectance (A_{Bt}) decreases for each succeeding row. Only the target size increases from the first to the second column.

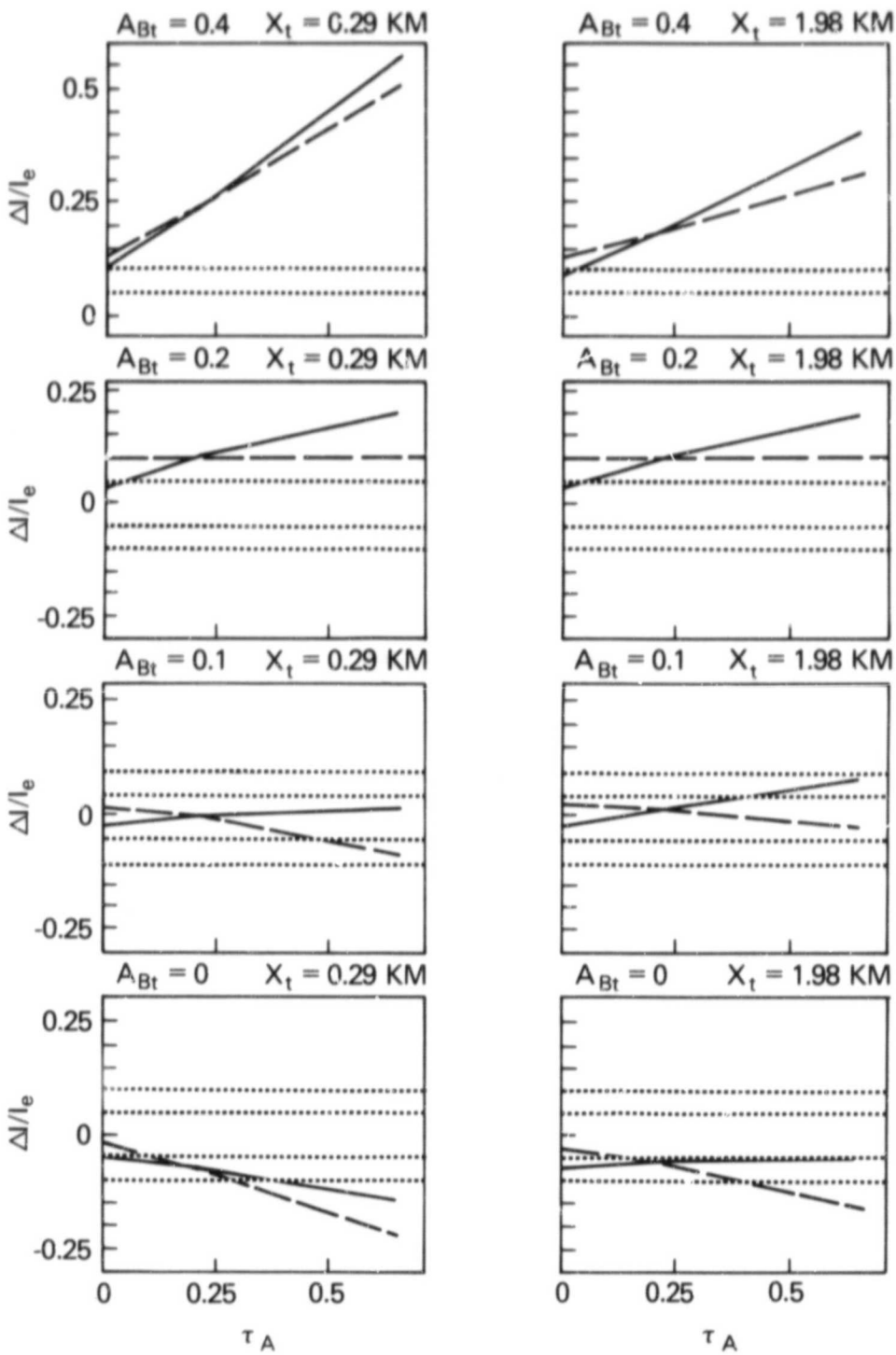

Figure 11. The relative change in radiance as function of the aerosol optical thickness without (solid line) and with uniform atmospheric correction (dashed line). Each row of graphs is given for a different ratio of A_{Bt}/A_t which changes for the respective rows from the bottom (0, 0.5, 1.0, 2.0). The left column is for A_r = 0.2, A_{Br} = 0.1, X_r = 0.29 km, T_r = 1, A_t = 0.2, X_t = 0.29 km. The right column is the same but for X_t = 1.98 km. The dotted lines give the ±5 and ±10% tolerance values of the difference in radiance.

A few general conclusions can be made regarding Fig. 11:

a. The radiance differences are negative, when the background reflectance is totally black ($A_{Bt} = 0$; bottom row).

b. The reflectances are the same ($\Delta I = 0$), where the reference and test regions are the same in the third row ($A_t = A_r = 0.2$ and $A_{Bt} = A_{Br} = 0.1$). The radiance difference depends slightly on turbidity in the third row, where the reference and test fields are the same size (left column). The difference increases to 8 percent where the field sizes are different.

c. The atmospheric correction for a uniform surface (dashed lines) does not change the difference between radiances of the reference and test areas, when the turbidity $T = 1$; but the difference increases for $T < 1$ and decreases for $T > 1$. The corrected and uncorrected radiance differences show the same tendency to lie outside of the tolerance limits. These limited data indicate that this atmospheric correction depending on turbidity does not reduce the absolute difference between the radiances of the test and reference fields, sufficiently to make a significant improvement in classification.

5. CLASSIFICATION SIMULATION

In this section we simulate the atmospheric effect on the radiance detected above agricultural regions consisting of the 15 classes given in Table 1. The simulated data are classified, and the

Table 1: Surface reflectance used in the simulation.

	BAND AND WAVELENGTH (nm)				
	4	5	6	7	
SURFACE	500-600	600-700	700-800	800-1100	REFERENCES
Soil	0.128	0.183	0.213	0.250	Deering (1981)
Alfalfa 30 kg/ha	0.117	0.155	0.228	0.305	Deering (1981)
Alfalfa 960 kg/ha	0.083	0.089	0.250	0.317	Deering (1981)
Alfalfa 1650 kg/ha	0.061	0.044	0.305	0.405	Deering (1981)
Alfalfa 2280 kg/ha	0.061	0.033	0.310	0.428	Deering (1981)
Alfalfa 3660 kg/ha	0.061	0.033	0.360	0.517	Deering (1981)
Alfalfa 3850 kg/ha	0.061	0.033	0.390	0.550	Deering (1981)
Water	0.010	0.009	0.004	0.003	Marsh and Lyon (1980)
Savanah	0.074	0.118	0.142	0.182	Kriebel (1977)
Bog	0.028	0.038	0.090	0.147	Kriebel (1977)
Pasture land	0.033	0.120	0.250	0.380	Kriebel (1977)
Coniferous land	0.014	0.024	0.044	0.116	Kriebel (1977)
Corn	0.072	0.060	0.320	0.540	Barker (1981)
Soybean	0.145	0.174	0.360	0.460	Barker (1981)
Wheat Stubble	0.066	0.100	0.134	0.175	Barker (1981)

Table 1-2: The normalized radiances are given above the atmospheric in the direction of the reference areas, which are used for classification. The atmospheric turbidity T = 1, and the edge length of the reference field of X = 1.23 km. The background for each reference area is soil.

	BAND AND WAVELENGTH (nm)			
	4	5	6	7
SURFACE	500-600	600-700	700-800	800-1100
Soil	0.1649	0.2068	0.2367	0.2653
Alfalfa 30 kg/ha	0.1559	0.1825	0.2465	0.3158
Alfalfa 960 kg/ha	0.1284	0.1258	0.2662	0.3268
Alfalfa 1650 kg/ha	0.1108	0.0875	0.3158	0.4087
Alfalfa 2280 kg/ha	0.1108	0.0782	0.3204	0.4302
Alfalfa 3660 kg/ha	0.1108	0.0782	0.3659	0.5146
Alfalfa 3850 kg/ha	0.1108	0.0782	0.3935	0.5462
Water	0.0702	0.0579	0.0505	0.0438
Savanah	0.1212	0.1505	0.1703	0.2035
Bog	0.845	0.0824	0.1247	0.1719
Pasture land	0.0884	0.1523	0.2662	0.3853
Coniferous forest	0.0734	0.0705	0.0849	0.1441
Corn	0.1186	0.1011	0.3294	0.5366
Soybean	0.1788	0.1990	0.3659	0.4605
Wheat Stubble	0.1148	0.1351	0.1632	0.1971

error of classification is analyzed for its dependence on fields size, background reflectance, and atmospheric turbidity.

The surface reflectances used in the simulation are given in Table 1 for wavelengths corresponding to the Landsat bands (band 4: 500-600 nm; 5: 600-700 nm; 6: 700-800 nm; 7: 800-1100 nm). The reflectances are interpolated from data given in the cited references. The atmospheric effects are derived from Pearce's (1977) Monte Carlo calculations of the radiance of finite fields, as they would be observed from a satellite. These radiances are rescaled according to the equations in Appendix 4, to account for the reflectances given in Table 1. In these simulations, the reference field and also the field to be classified are square and surrounded by a uniform background of different reflectance.

An extrapolation of Pearce's (1977) radiances for 550 nm to other wavelengths is required, also. The wavelength dependence is expressed by means of the total, normal optical thickness of the atmosphere ($\tau_o = \tau^R + \tau^A$). The optical thicknesses are calculated with respect to the optical thicknesses of particles (τ^A) and molecules (τ^R) at 500 nm from the following relations:

$$\tau^R(\lambda) = \tau^R(550)\ (\lambda/550)^{-4.09}$$

$$\tau^A(\lambda) = \tau^A(550)\ (\lambda/550)^{-\nu} \qquad (10)$$

where ν is calculated from Pearce's data (1977) as $\nu = 0.97$. The

rescaling of the radiances to account for different optical thicknesses is given in Appendix 4. The reference square fields are taken here always with a size of 1.23 km, and for average atmospheric turbidity of 1. Table 2 gives the radiances for the different reference fields with a background of soil.

The classification of an unknown (test) field is performed by associating it with the reference field giving a minimum radiance difference defined by:

$$\epsilon_k^2 = \frac{1}{4} \sum_{i=1}^{4} (I_{ti} - I_{ri}^k)^2 \qquad k = 1, 2, \ldots, 15 \qquad (11)$$

where I_{ti} and I_{ri} are the radiances above the center of the test and reference fields, respectively. The superscript k ranges through the complete set of integers from 1 to 15, corresponding to the 15 classes listed in Table 1. The turbidity is always one (T = 1) for the 15 reference fields and their size is always X_r = 1.23 km.

The classification results are given in Figs. 12a, b, and c. The table at the top of each figure gives details about the fields and their backgrounds used in the simulation. The atmospheric turbidity is given in the column labeled T. Column C indicates by the word "yes" the data after an atmospheric correction is applied. The correction is made for a surface of uniform reflectance. The fields are designated by a letter: R for reference field, T for test field, C for the test field after the atmospheric correction has been applied, and A, B for the one or two fields that have the closest

"a"

The effect of turbidity alone

	FIELD OF	FIELD ON	X (KM)	T	C	RADIANCE FOR LANDSAT DATA 4	5	6	7	CLASSIFIED AS
T	Coniferous Forest	Soil	1.23	3		.125	.118	.126	.171	Wheat Stubble
R	Coniferous Forest	Soil	1.23	1		.073	.070	.085	.144	-
C	Coniferous Forest	Soil	1.23	3	Yes	.092	.091	.104	.156	Bog
A	Bog	Soil	1.23	1		.084	.082	.125	.172	-
B	Wheat Stubble	Soil	1.23	1		.115	.135	.163	.197	-

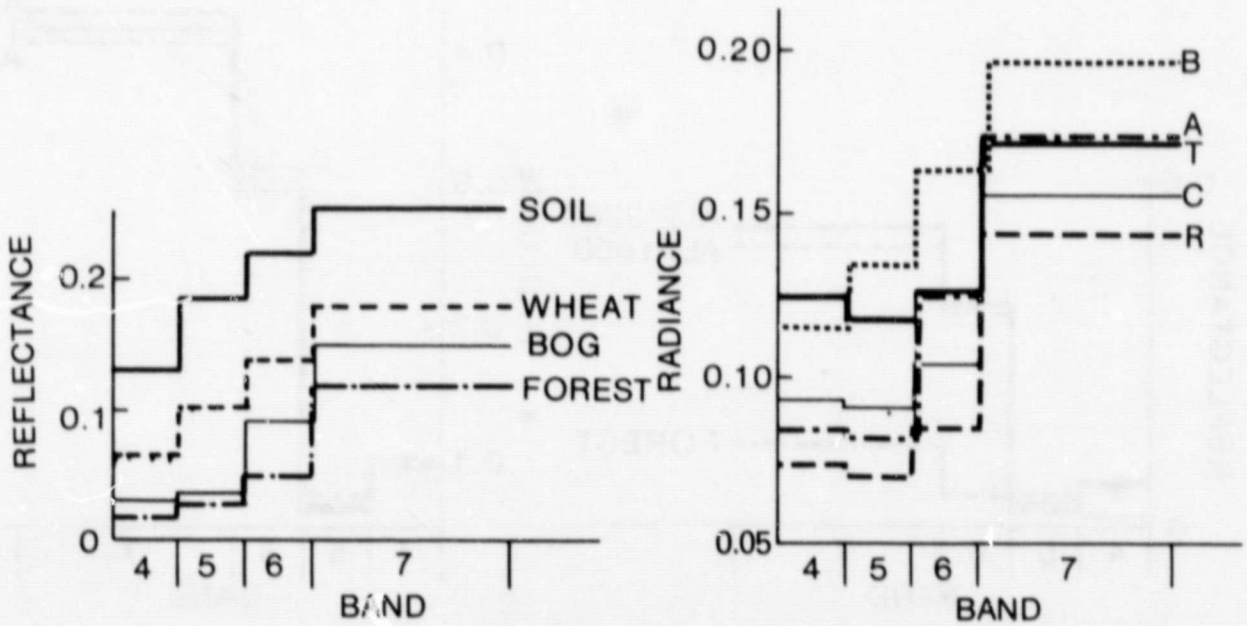

Figure 12. Examples of atmospheric effect on classification: a - The effect of turbidity alone; b - The effect of size alone; c - Combined effect; and d - Classification of water. Each example gives the radiances of the fields both in tabular and graphical form. In addition, the reflectance of each cover is given.

"b"
The effect of size alone

	FIELD OF	FIELD ON	X (KM)	T	RADIANCE FOR LANDSAT BAND 4	5	6	7	CLASSIFIED AS
T	Alfalfa 2280	Coniferous Forest	0.111	1	.097	.066	.297	.411	Alfalfa 1650
R	Alfalfa 2280	Coniferous Forest	1.23	1	.101	.066	.309	.423	-
A	Alfalfa 1650	Coniferous Forest	1.23	1	.101	.075	.305	.402	-

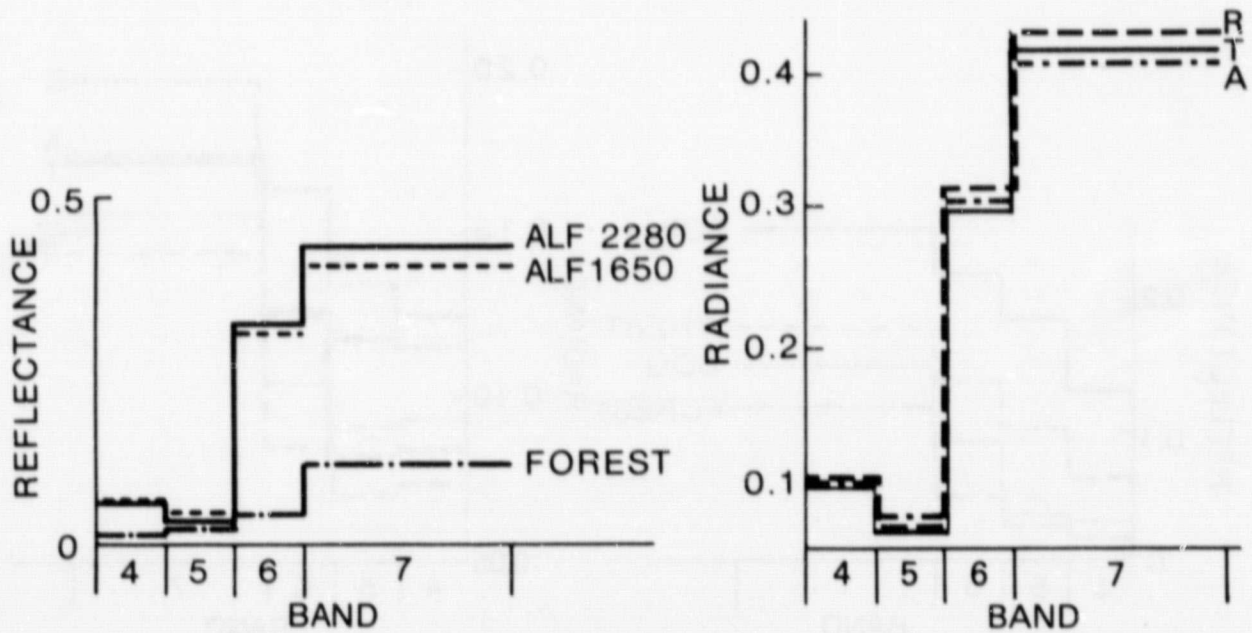

Figure 12 (continued)

"c"

Combined effect

	FIELD OF	FIELD ON	X (KM)	T	C	RADIANCE FOR LANDSAT BAND 4	5	6	7	CLASSIFIED AS
T	Wheat Stubble	Coniferous Forest	0.111	3		.122	.130	.153	.194	Wheat Stubble
R	Wheat Stubble	Soil	1.23	1		.115	.135	.163	.197	-
C	Wheat Stubble	Coniferous Forest	0.111	3	Yes	.088	.104	.133	.180	Bog
A	Bog	Soil	1.23	1		.088	.082	.125	.172	-

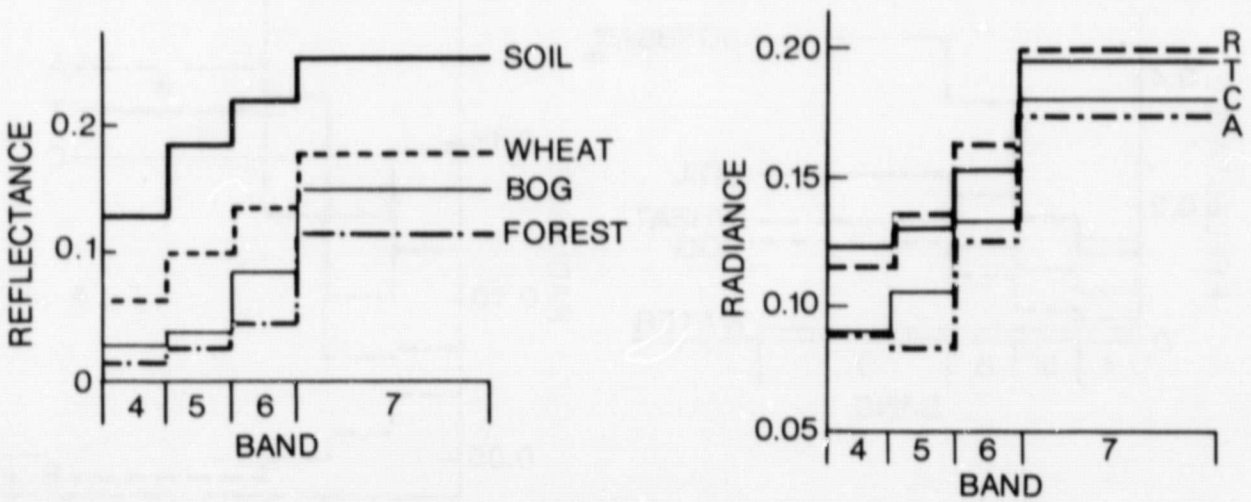

Figure 12 (continued)

"d"
Classification of water

	FIELD		X	T	C	RADIANCE FOR LANDSAT BAND				CLASSIFIED
	OF	ON	(KM)			4	5	6	7	AS
T	Water	Soybean	0.111	3		.147	.127	.164	.159	Wheat Stubble
R	Water	Soil	1.23	1		.070	.058	.050	.044	-
C	Water	Soybean	0.111	3	Yes	.115	.101	.145	.144	Bog
A	Bog	Soil	1.23	1		.084	.082	.125	.172	-
B	Wheat Stubble	Soil	1.23	1		.115	.135	.163	.197	-

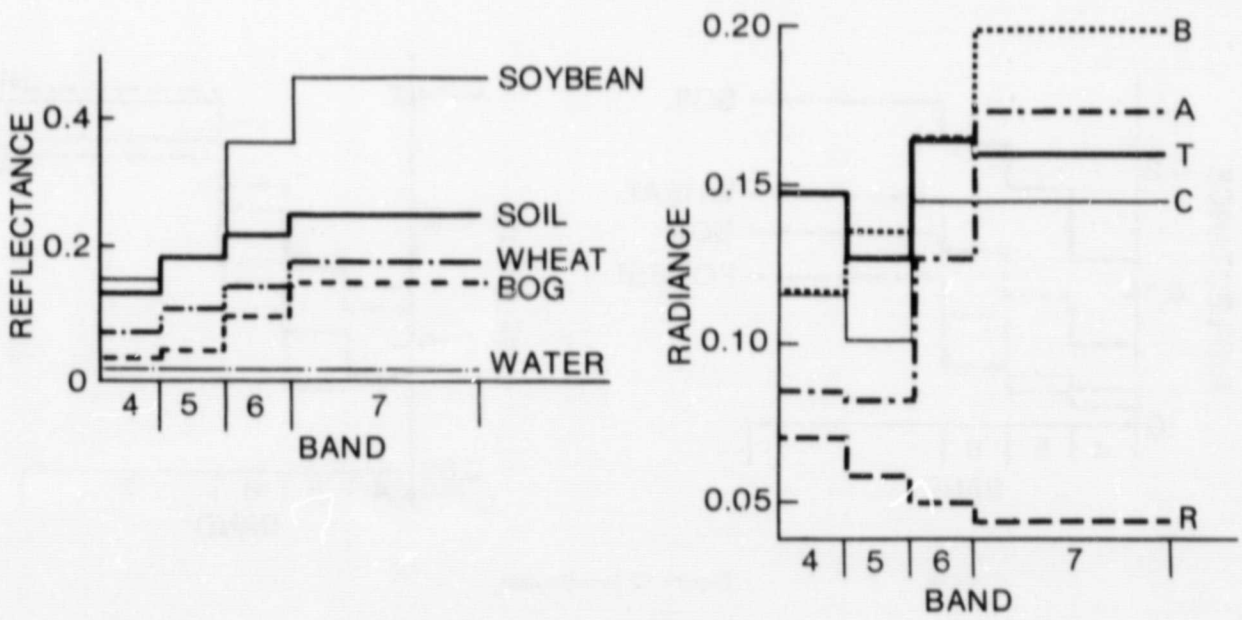

Figure 12 (continued)

spectral characteristics to fields T and C. The reflectances of the fields at the surface are shown in the lower left figure. The radiances above the atmosphere are taken from the table and reproduced in the lower right figure.

Only the atmospheric turbidity changes between the reference (T = 1) and test (T = 3) fields in Fig. 12a. The edge length of all fields in the simulation is X = 1.23 km. The reference and test fields are coniferous forests surrounded by a background of soil. Because the radiances above the test field are higher than those of the reference field, the forest is misclassified as wheat stubble (B). The corrected data (C) is classified as bog (A). In actuality, the atmospheric turbidity does not usually vary so strongly between reference and test fields, but when it does, serious classification errors arise.

The field size is the only parameter that changes between the reference (X_t = 1.23 km) and the test (X_r = 0.11 km) fields for Fig. 12b. The fields are alfalfa of density 2280 kg/ha with backgrounds of coniferous forest. The test field is still classified as alfalfa, but of lower density (1650 kg/ha). The size difference results in a misclassification, even though the atmospheric characteristics and the surface reflectances are the same for both the reference and test regions.

In Fig. 12c the combined effect of turbidity, background reflectance, and size is examined. The test field is wheat stubble on

a background of coniferous forest, for X_t = 0.111 km and T_t = 3. A comparison of the radiances of this test field with a reference field of wheat stubble shows that the atmospheric effect is weak in this case due to the relatively dark background. Therefore the field is classified correctly as wheat stubble. The atmospheric effect would be much stronger for a uniform field of wheat stubble; thus, the resultant uniform atmospheric correction to the radiances in (T) results in a decrease of the radiances to the result shown in (C). This decrease is caused by the uniform atmospheric correction, which does not account for the adjacency effect. The result of this correction is that the field is misclassified as bog (A). This example shows how uniform atmospheric correction can cause a misclassification of data that were classified correctly before.

An example of classification of water basins is shown Fig. 12d. A square water pond of 0.111 km on a side with a background of soybeans for T = 3 is misclassified as wheat stubble due to the large increase of radiances from line R to line T. The uniform atmospheric correction causes here only a slight correction, and the water pond is still misclassified, this time as bog. This example shows that small reservoirs of water on bright backgrounds can be misclassified from space, and a uniform atmospheric correction cannot provide an adequate correction.

6. CONCLUSIONS

The simulation study presented in this paper shows that

nonuniform reflectance of the earth's surface results in an important modification of effect of the atmosphere on remote sensing of the surface and thus on classification of surface features. The adjacency effect, which increases the radiance detected above dark fields surrounded by adjacent bright areas (and vice versa) creates an atmospheric effect, which cannot be corrected by methods utilizing a uniform surface. Therefore, future development of atmospheric correction algorithms has to account for the nonuniform nature of the earth's surface.

APPENDIX 1

List of notations frequently used in the paper.

A. Surface reflectances

A_a - Average of reflectance of both a field and its background for calculation of the multiple scattering of light between the surface and the atmosphere.

A_B - Background reflectance (reflectance of the area surrounding a field).

A_{Bt}, A_{Br} - Background reflectance for the test and reference fields, respectively.

A_D - Weighted average of the surface reflectance of the entire surface for calculation of the diffuse transmission through the atmosphere.

A_f - Reflectance of a given field.

A_r - Reflectance of a reference field.

A_S - Reflectance of the surface within IFOV.

A_t - Reflectance of a test field.

B. Radiances

I^* - Absolute radiance.

I - Normalized radiance equivalent to the apparent reflectance and given by $I = \pi I^*/(\mu_o F_o)$.

I_D - Radiance transferred diffusively through the atmosphere from the surface to a detector.

I_e - The radiance which would be measured if no atmosphere

were present.

I_0 - Radiance of light scattered from the direct solar beam into the detector field of view without being scattered by the surface.

I_S - Radiance of light reflected by the observed field and directly transmitted through the atmosphere.

I^u - Radiance above uniform surface.

I^n - Radiance above nonuniform surface.

C. Other notations

T_r - Atmospheric turbidity above the reference field.

T_t - Atmospheric turbidity above the test field.

X_r - Edge length of the reference field.

X_t - Edge length of the test field.

γ_o - The total transmission of the sunlight to the surface.

D - Diffuse transmission through the atmosphere.

τ_o - Total atmospheric optical thickness ($\tau^A + \tau^M$).

τ^A - Aerosol optical thickness.

τ^M - Molecular optical thickness.

APPENDIX 2 - APPLICATION OF DAVE'S CODE

The equations giving the radiance above the center of an infinitesimally small square lying on a uniform background are derived. Chandrasekhar (1960), gave an equation for the upward radiance above an atmosphere on a uniform surface that reflects light according to Lambert's law:

$$I^u = I_0 + \frac{\gamma_o}{1 - \ell A} \quad (EA \cdot DA) \qquad (2\text{-}1)$$

where E is the direct upward transmittance by the atmosphere. In the case of a small object of reflectance, A_t laying on a background of reflectance A_B, the upward radiance is given by:

$$I\ (A_t,\ A_B,\ T,\ X \to 0) = I_0 + \frac{\gamma_o}{1 - \ell A_B}\ (EA_t + DA_B) \qquad (2\text{-}2)$$

Equation (2-2) is obtained from Eq. (2-1) by substituting A_t for the reflectance in the term of direct transparency, and A_B for terms of diffuse transparency and reflection. This can be done as long as the object is not big enough to affect the diffuse component (edge length << 300 m). Dave's results for an infinitesimal field and an infinitesimal field of view of the detector are compared with the Monte Carlo calculations for a finite field of view of footprint of 30 m and object field of edge length of 40 m (Figs. 5 and 6). The differences shown in Figs. 5 and 6 are partially due to the finite sizes of the footprint and the object field and in addition can be due to computational errors or small differences between the atmospheric model used in the Monte Carlo

calculations and in the Dave calculations.

The small differences do not introduce significant errors in the adjacency effects, because of the wide range of latter (Mekler and Kaufman, 1980). Thus, Pearce's data are reliable for studies of the adjacency effects.

APPENDIX 3 - PROPORTIONAL RADIANCE TRANSFORMATION

The equations that are used to transform the radiances from the values in Figs. 5 and 6 for one set of surface reflectances to new radiances for different sets of surface reflectances are derived in this appendix. These equations are use to calculate the data on Figs. 7-8 and 10-11. The radiance at the center of a square of reflectance A_t of any edge length (X) can be formally given by (see Eq. 5):

$$I\ (A_t,\ A_B,\ T,\ X) \;=\; I_0 \;+\; \frac{\gamma_o}{1 - \ell A_a}\ (EA_t \;+\; DA_D) \qquad (3\text{-}1)$$

where $E = (\exp\ (-\tau_o))$, A_a and A_D are reflectances obtained as weighted average of the reflectance of the square and its background:

$$\begin{aligned} A_a &= \alpha_a\ A_t \;+\; (1 - \alpha_a)\ A_B \\ A_D &= \alpha_D\ A_t \;+\; (1 - \alpha_a)\ A_B \end{aligned} \qquad (3\text{-}2)$$

where α_a and α_D depend on the atmospheric optical characteristics. α_a and α_D can be expressed as complex solutions to the radiative transfer equation. We shall not find these solutions here but express α_D by using the Monte Carlo data; and we shall roughly estimate the value of α_a. Rough estimation of α_a does not cause a significant error in Eq. (3-1), since the term (ℓA_a) is relatively small. In the present work $\ell \leq 0.2$, affecting the final radiance by 0-10 percent. Thus, an error in α_a of 10-20 percent causes an error in the radiance of 0-2 percent.

The transformation from known values of I for a set of reflectances (A_t, A_B) to new values of I for another set (A_t', A_B') is given by:

$$I(A_t', A_B', T, X) = \left\{ I\left[(A_t, A_B, T, X) - I_o\right] \cdot R_A \right\} \cdot \left(\frac{1 - \ell A_a}{1 - \ell A_a R_a}\right) + I_o \tag{3-3}$$

The data in Figs. 7-8 and 10-11 are calculated for:

$$R_A = \frac{A_t'}{A_t} = \frac{A_B'}{A_B} \tag{3-4}$$

This ratio has been used to obtain the simplified expression (3-3). In this transformation, the linear dependence of the radiance on surface reflectance is transformed exactly, while on the nonlinear part $(1 - \ell A_a)$ an approximate transformation was applied using the following expression for A_a:

$$A_a = A_t \left[1 - e^{-\left(\frac{X}{R}\right)^2} \right] + A_B \; e^{-\left(\frac{X}{R}\right)^2} \tag{3-5}$$

where X is the edge length. The value of R = 6 km is found to give good results and is used in the calculations. This approximate expressions might introduce errors in A_a of ($\Delta A_a = \pm 0.1$). Since the value of ℓ used in the present paper is $\ell \leq 0.21$, the resultant error in radiance is less than 2 percent.

APPENDIX 4 - GENERAL RADIANCE TRANSFORMATION

In this appendix we shall explain the transformation applied to the radiance $I(A_t, A_B, \tau^A, \tau^M, X)$ above a square of reflectance A_t and edge length X lying on a background of reflectance A_B and for optical thicknesses τ^A and τ^M to obtain another radiance for a new set of parameters A_t^*, A_B^*, τ^{A*} and τ^{M*}, giving $I(A_t^*, A_B^*, \tau^{A*}, \tau^{M*}, X)$. The transformation is done in two steps. First, the transformation is made with respect to surface reflectances and then transformation for the optical thickness. The transformation for the surface reflectances is done by Eqs. (3-1) and (3-2). Substituting A_D from Eq. (3-2) into Eq. (3-1), we find that :

$$I(A_t, A_B, \tau^A, \tau^M, X) = I_0 + \frac{\gamma_o}{1 - \ell A_a} A_t (E + D\alpha_D) + A_B D (1 - \alpha_D) \qquad (4\text{-}1)$$

For a uniform surface of reflectance A_t, we can rewrite Eq. (2-1) in the form:

$$I^u(A_t) = I_0 + \frac{\gamma_o}{1 - \ell A_t} (EA_t + DA_t) \qquad (4\text{-}2)$$

From Eqs. (4-1) and (4-2) we can write:

$$I(A_t, A_B, \tau^A, \tau^M, X) = I^u(A_t) + \gamma_o E A_t G_1 + C \left(\frac{A_B - G_2 A_t}{1 - \ell A_a}\right) \qquad (4\text{-}3)$$

where: $C = \gamma_o D (1 - \alpha_D)$

$$G_1 = \frac{\ell\,(A_a - A_t)}{(1 - \ell A_a)\,(1 - \ell A_t)}$$

$$G_2 = 1 + \frac{\ell\,(A_t - A_a)}{1 - \ell A_t}$$

Expression (4-3) can be simplified by neglecting terms of the order of $(\ell\Delta A)$. This approximation was found to introduce an error of 0-4 percent in the resulting radiances for the present calculations. The resultant coefficients are $G = 0$ and $G_2 = 1$. Hence

$$I\,(A_t, A_B, \tau^A, \tau^M, X) = I^u\,(A_t) + C\,\frac{A_B - A_t}{1 - \ell A_a} \qquad (4\text{-}4)$$

The transformed radiance:

$$I\,(A_t^*, A_B^*, \tau^A, \tau^M, X) = I^u\,(A_t) + C\,\frac{A_B^* - A_t^*}{1 - \ell A_a'} \qquad (4\text{-}5)$$

is calculated by using C from Eq. (4-4) for the known value of $I(A_t, A_B, \tau^A, \tau^M, X)$, and using A_a and A_a' from Eq. (3-5). The value of $I_{A_t}^*$ was calculated from I_{At}, I_0 and know value of ℓ by Eq. (4-2).

The transformation on the optical thickness is based on the following assumptions.

a. The radiance is both linear on the aerosol and molecular optical thickness.

b. It is possible to separate the dependence of the radiance on the aerosol optical thickness from its dependence on the molecular optical thickness.

c. Mathematically, these assumptions allows us to express the the radiance by:

$$I\ (\tau^A,\ \tau^M) \ = \ i_0 \ + \ i_A \tau^A \ + \ i_M \ \tau^M \qquad (4\text{-}6)$$

Table (4-1) shows examples of the radiances calculated by Eq. (4-6) from radiances at other optical thicknesses, and compared with radiances obtained directly. The edge length of the square (X) for which the radiance is given is also tabulated, in addition to the values of A_t an A_B.

Equation (4-6) can be used to transform the radiance to new values of optical thickness by:

$$I\ (\tau^{A*},\ \tau^{M*}) \ = \ I\ (0,\ \tau^M) \ - \ A_t \ \frac{\tau^{M*}}{\tau^M} \ + \qquad (4\text{-}7)$$

$$I\ (\tau^A,\ \tau^M) \ - \ I\ (0,\ \tau^M) \ \frac{\tau^{M*}}{\tau^M} \ + \ A_t$$

Table 4-1: Comparison between radiances obtained by Figs. (4-6) and radiances calculated directly.

			RADIANCES USED IN FIGS.(4-6)				
X(KM)	A_C	A_B	$\tau^M=0$ $\tau^A=0$	$\tau^M=0.1$ $\tau^A=0$	$\tau^M=0.10$ $\tau^A=0.21$	RESULTANT RADIANCE $\tau^M=0.1$, $\tau^A=0.637$	RADIANCES OBTAINED DIRECTLY
1.23	0.4	0.2	0.4	0.391	0.381	0.361	0.366
0.179	0.6	0.0	0.6	0.544	0.479	0.349	0.354
0.47	0.2	0.4	0.2	0.229	0.256	0.310	0.315
0.758	0.0	0.6	0.0	0.063	0.120	0.234	0.250
∞	0.0	-	0.0	0.039	0.051	0.075	0.088
∞	0.2	-	0.2	0.218	0.231	0.257	0.251
∞	0.4	-	0.4	0.405	0.408	0.414	0.420
∞	0.6	-	0.6	0.596	0.601	0.611	0.605

REFERENCES

Barker, J, 1981: Private communication.

Chandrasekhar, S., 1960: Radiative transfer. Dover, New York, p. 273.

Dave, J. V. and J. Gazdag, 1970: A Modified Fourier Transform Method for Multiple Scattering Calculations in a Plane-Parallel Mie Atmosphere, Appl. Opt., 9, 1457-1466.

Dave, J. V., 1980: Effect of atmospheric conditions on remote sensing of a surface nonhomogenity. Photog. Eng. and Rem. Sen., 46, 1173.

Fraser, R. S., 1974: Computed atmospheric corrections for satellite data. Proc. of the SPIE Conference on Scanners and Imagery Systems for Earth observation, SPIE, 51, 64.

Fraser, R. S., Bahethi, Om P. , and Al-Abbas, A. H. 1977: The effect of the atmosphere on classification of satellite observations to identify surface features. Remote Sensing of Environment, 6, 229.

Griggs, M., 1973: A method to measure the atmospheric aerosol content using ERTS-1 data. Proc. of the Third ERTS-1 symposium, NASA Sp-351, pp. 1505.

Griggs, M, 1979: Satellite observations of atmospheric aerosols during the EOMET cruise. J. Atmos. Sci., 36, 695.

Haba, Y., Kawata, Y., Kusaka, T., and Uneo, S., 1979: The system of correcting remotely sensed earth imagery for atmospheric effects. Proc. of the 13 Int Symp. on Remote Sensing of Environment, Ann Arbor, Michigan, pp. 1883.

Herman, B. M. and Browning, S. R., 1975: The effect of aerosols on the earth-atmosphere albedo. J. Atmos. Sci., 32, 1430.

Horvath, R. B., Polcyn, J. G., Fabian, C., 1970: Effects of atmospheric path on airborne multispectral sensors. Remote Sensing of Environment, 1, 203.

Kaufman, Y. J. and Joseph, J. H., 1981: Evaluation of surface albedos and extinction characteristics of the atmosphere from satellite iamges. Accepted for publication in J. Geophys. Res.

Kawata, Y., Haba, Y., Kusaka, T., Terashita, Y., and Ueno, S., 1978: Atmosphere effects and their correction in airborne sensor and Landsat MSS data. Paper presented at Proceedings of the 12th International Symposium on Remote Sensing of Environment, ERIM, Ann Arbor, Michigan.

Kriebel, K. T., 1977: Reflection properties of vegetated surfaces:

tables of measured spectral biconical reflectance factors, Universitat Munchen, Wissenschaftliche Mitteilung, No. 29, Munchen, W. Germany.

Labovitz, M. L., Toll, D. L., and Kennard, R. E., 1980: Preliminary evidence for the influence of Physiography and scale upon the autocorrelation function of remotely sensed data, NASA TM 82064, NASA/Goddard Space Flight Center.

Marsh, S. E. and Lyon, R. J. P., 1981: Quantitative relationships of near surface spectra to Landsat radiometric data. Remote Sensing of Environment, 10, 241.

Mekler, Y. and Kaufman, Y. J., 1980: The effect of earth's atmosphere on contrast reduction for a nonuniform surface albedo and two halves field. J. Geophys. Res., 85, 4067.

Mekler, Y., Quenzel, H., Ohring, G., and Marcus, I., 1977: Relative atmospheric aerosol content from ERTS observations. Geophys. Res., 82, 967.

Otterman, J. and Fraser, R. S., 1976: Earth-atmosphere system and surface reflectivities in arid regions from Landsat MSS data. Remote Sensing of Environment, 5, 247.

Otterman, J. and Fraser, R. S., 1979: Adjacency effects on imaging by surface reflection and atmospheric scattering: Cross-irradiance to zenith. Appl. Opt., 18, 2852.

Pearce, W. A., 1977: A study of the effects of the atmosphere on thematic mapper observations. Rep. 004-77, EG&G/Washington Anal. Serv. Center, Appl. Sys. Dep., Riverdale, Maryland, 136 pp.

Peterson, J. T., Flowers, E. C., Berri, G. J., Beynolds, C. L., and Rudisill, J. H., 1981: Atmospheric turbidity over Central North Carolina. J. Appl. Met., 20, 229.

Pitts, D. E. and Badhwar, G., 1980: Field size, length, and width distributions based on LACIE Ground Truth data. Remote Sensing of Environment, 10, 201.

Potter, J. F., 1976: Correcting landsat data for changes in sun angle, haze level, and background reflectance. Proc. of the 1976 machine processing of remotely sensed data symposium. IEEE 76CH 1103-IMPRSD, 2B-6.

Richard, P. R., 1979: Determination of noise equivalent reflectance for a multispectral scanner - a scanner sensitivity study, NASA Tech. paper, NASA Lyndon B. Johnson Space Center, 1575.

Richard, P. R., 1981: Private communication.

Schowengerdt, R. A. and Slater, P. N., 1979: Literature survey and review of atmospheric effects in remote sensing and their

influence on classification. ORI, Inc. 1400 Spring Street, Silver Spring, Maryland, 20910.

Slater, P. N., 1980: Atmospheric corrections using an orbital, pointable imaging system. ORI Inc., 1400 Spring Street, Silver Spring, Maryland, 20910.

Turner, R. E. and Spencer, M. M., 1972: Atmospheric model for correction of spacecraft data. Proc. of the Eighth International Symposium on Remote Sensing of Environment, ERIM, October, 1972, pp. 895-934.

Turner, R. E., 1978: Elimination of atmospheric effects from remote sensor data. Proc. of the 12th International Symposium on Remote Sensing of Environment, ERIM, pp. 783.